

RESEARCH ARTICLE

# A partial compensation scheme for MMC-based railway cophase power supply

Peiliang Sun, Kang Li\* and Chen Xing

School of Electronic and Electrical Engineering, University of Leeds, LS2 9JT, Leeds, UK

\*Corresponding author: E-mail: [K.Li1@leeds.ac.uk](mailto:K.Li1@leeds.ac.uk)

## Abstract

This paper presents a partial compensation scheme for V/v transformer cophase traction power supply in high-speed railway systems. The scheme compensates variable traction load current, and controls the current phase at the secondary side of the V/v transformer for power factor correction and negative sequence current reduction. To achieve this, the grid side current phase angles are optimized while satisfying the grid code on the power factor and voltage unbalance limits. The optimized phase angles are then used to design control references under varying load conditions. The compensation control action is updated regularly based on real-time measurements of the traction load, and the required currents are controlled by a 25-level single-phase back-to-back MMC power conditioner to achieve the compensation target. Static and dynamic load compensation performances are verified based on the simulation studies.

**Keywords:** railway power supply; cophase supply; modular multilevel converter; V/v transformer compensation; power quality

## Nomenclatures

$\check{I}^+, \check{I}^-, \check{I}^0$ : Current phasors of positive sequence, negative sequence and zero sequence components $\check{U}, \check{I}$ : Voltage phasor and current phasor $pf_A, pf_B, pf_C$ : Power factors at the grid side $pf_{Tr}$ : Power factor of the traction load $\phi_{Tr}$ : Phase angle of the traction load current phase lagging to its supply voltage	$\varphi_A, \varphi_B, \varphi_C$ : Phase angles of three-phase currents lagging to the supply voltage at the grid side $I_{aa}, I_{cc}$ : RMS (Root-Mean-Square) current values at the secondary sides of the feeder station transformer $I_A, I_B, I_C$ : RMS values of three-phase current at the grid side of the feeder station transformer
--	--

Received: 30 March 2020; Revised: 4 June 2020; Accepted: 23 June 2020

© The Author(s) 2020. Published by Oxford University Press on behalf of Central South University Press. This is an Open Access article distributed under the terms of the Creative Commons Attribution License (<http://creativecommons.org/licenses/by/4.0/>), which permits unrestricted reuse, distribution, and reproduction in any medium, provided the original work is properly cited.

$I_{Tr}$ :	RMS value of the traction load current
$N$ :	Transformer turns ratio
$U_{ab}, U_{cb}$ :	RMS values of the V/v transformer secondary side voltage
$U_A, U_B, U_C$ :	RMS values of three-phase voltage at the grid side of the feeder station transformer

## 1. Introduction

Three electrified railway traction power supply solutions are widely used, namely the 16 2/3 Hz 15 kV ac system, 50 Hz 25 kV ac system and 3 kV dc system. Among them, 25 kV 50 Hz ac traction power supply is most popular and in such a system, the feeder station converts three-phase power supply (often at 110 kV) from the distribution network to single-phase power supply (often at 25 kV) feeding to the railway overheadline (Fig. 1a). To step down the voltages, V/v (V/x) transformers with autotransformer connection are widely used in high-speed railway systems [1]. These transformers generate two single-phase voltage sources for two traction supply arms, which however inevitably introduces power unbalance and low power factor current into the grid, causing power quality issues. Furthermore, these transformers lack the ability to suppress harmonic currents produced by variable traction loads.

To address these issues from the power source perspective, improved transformers with special connection topologies have been developed and installed to reduce the negative sequence issue, such as the Scott transformer and Woodbridge transformer, which can eliminate negative sequence current provided that both sides are equally loaded [2]. However non-balance transformers like I/i, V/v and YNd11 cannot eliminate negative sequence current even when the loads at two sides are perfectly balanced, unless certain reactive current is added externally [3].

Another approach to improve the traction power quality is to use additional devices to compensate reactive power, negative sequence current and harmonics. Various types of compensators for railway applications are intensively researched [4–7]. This equipment can be installed either at the grid side of the feeder stations or at the traction power supply side.

Since the 2010s, many power electronics-based compensators have been used directly on the traction power network side for power quality conditioning. These converters in various forms include railway power regulators, active power quality compensators (APQCs), railway power conditioners (RPCs), power quality conditioners (PQCs), power flow controllers (PFCs), etc. Their topologies fall into two categories: power quality conditioning between two supply arms (Fig. 1b), and combining two arms into one as a cophase system (Fig. 1c). Both topologies can balance the grid side current, but the cophase system has the advantage of reducing or even eliminating the neutral sections [8].

In the existing solutions, large LC impedance matching filters and transformers are needed for connection between converters and transformers. In [6], a special design is investigated to reduce the dc-link voltage via coupling impedance in which the reactive power is absorbed by the passive filter; however, this is only applicable in certain current load conditions. Chen et al. use a magnetic static var compensator (MSVC) to dynamically change impedance in response to the locomotive load variations [7]. Although the passive impedance can reduce the conditioner's voltage rating, the MSVC cannot follow rapid load change perfectly. Power electronics-based compensators still have to provide some reactive power.

Cophase conditioners proposed in the literature are operated with a fixed compensation strategy or under the minimum active power capacity criteria. However, these approaches cannot fully minimize the loss when the traction load is lower than the nominal capacity of the conditioning system. Additionally, existing proposals use a bang-bang (hysteresis) controller for compensation current tracking control which may not be an acceptable option. Because the switching frequency is not directly constrained and a high switching frequency is required to achieve good performance, the bang-bang control is hardly suitable for real applications nor for the multilevel converters.

This paper investigates the V/v transformer-based cophase supply scheme, and employs single-phase 25-level half-bridge modular multilevel converter (MMC) back-to-back topology to enable direct connection to the traction network without transformer or additional passive filters. Compensation current reference is calculated in real time to satisfy different load variations. The converter is controlled by proportional resonant (PR) controllers for current tracking, and

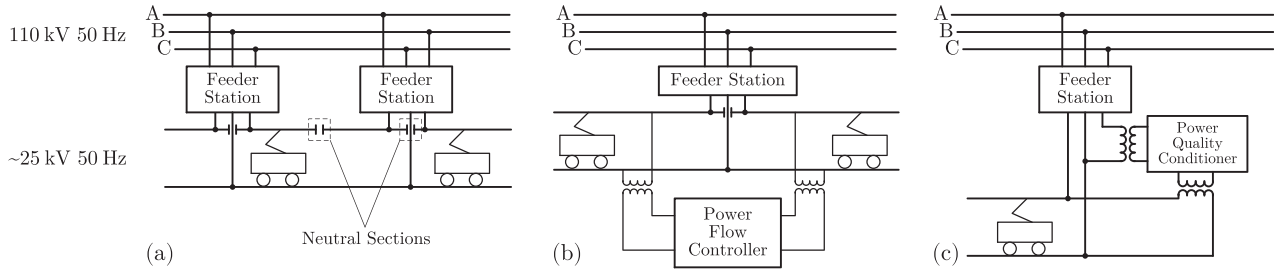


Fig. 1. Railway traction power supply structures (a) and active power quality controller configurations (b) power quality conditioning between two supply arms; (c) a cophase system

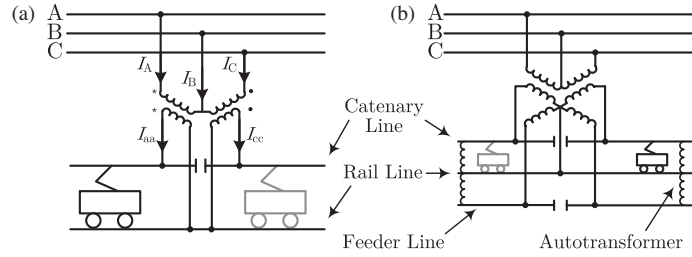


Fig. 2. V/v transformer (a) and V/x transformer feeder station (b)

carrier wave phase-shifted pulse width modulation (CPS-PWM) is adopted to control the states of switches. The remainder of the paper is organized as follows. Section 2 presents the preliminaries in regards to the V/v transformer feeder station and discusses the corresponding power quality issues. Section 3 details the compensation strategy design. Section 4 describes the control scheme for the MMC power conditioner. Sections 5 and 6 analyse the comprehensive simulation results and conclude the paper.

## 2. V/v transformer feeder station and the inherent power quality issues

The wiring diagrams of the V/v and V/x transformer are illustrated in Fig. 2. There are two single-phase transformers connecting phase AB and phase CB, and these types of transformers are widely used in current railway systems. The V/x transformer is similar to V/v wiring type and can cancel the autotransformer (AT) within the feeder station. To make the following analysis easier to follow,  $\check{I}_{bb}$  (a virtual current at the transformer secondary side) is used. The relation of the currents at both sides of the transformer is expressed in equation (1).

$$\begin{cases} \check{I}_{aa} = N\check{I}_A \\ \check{I}_{cc} = N\check{I}_C \\ \check{I}_{bb} = -(\check{I}_{aa} + \check{I}_{cc}) = N\check{I}_B \end{cases} \quad (1)$$

To facilitate the analysis,  $\check{I}_{aa}$ ,  $\check{I}_{bb}$  and  $\check{I}_{cc}$  are used to represent the three-phase current condition at the grid side. The phasor diagram of V/v transformer with three different load conditions is illustrated in Fig. 3: (a) single-side load, (b) both sides with equal load and (c) one side half loaded more than the other side.  $I_{TrL}$  and  $I_{TrR}$  are the traction load current RMS values on the left supply arm and on the right supply arm respectively. Due to different voltage phases of the two supply arms, a neutral section is necessary inside each feeder station. The existence of a neutral section blocks the energy sharing between the two supply arms and introduces a no-power zone where the train has to rely on inertia and on-board energy sources without external supply.

Another issue is the inevitable negative sequence current, no matter how balanced the traction loads are in each supply arm. As shown in Fig. 3, the three-phase current unbalance is most severe when only one side is loaded (Fig. 3(a):  $I_{aa} = I_{bb} = I_{Tr}$ ,  $I_{cc} = 0$ ) and is lightest when both sides are equally loaded (Fig. 3(c):  $I_{aa} = I_{cc} = I_{Tr}$ ,  $I_{bb} = \sqrt{3}I_{Tr}$ ). The grid side negative sequence components are calculated by transforming the three unbalance current phasors into three sets of symmetric phasors by equation (2).

$$\begin{bmatrix} \check{I}^0 \\ \check{I}^- \\ \check{I}^+ \end{bmatrix} = \frac{1}{N} \begin{bmatrix} 1 & 1 & 1 \\ 1 & \alpha^2 & \alpha \\ 1 & \alpha & \alpha^2 \end{bmatrix} \begin{bmatrix} \check{I}_{aa} \\ \check{I}_{bb} \\ \check{I}_{cc} \end{bmatrix}, \quad \alpha \equiv e^{+j120^\circ} \quad (2)$$

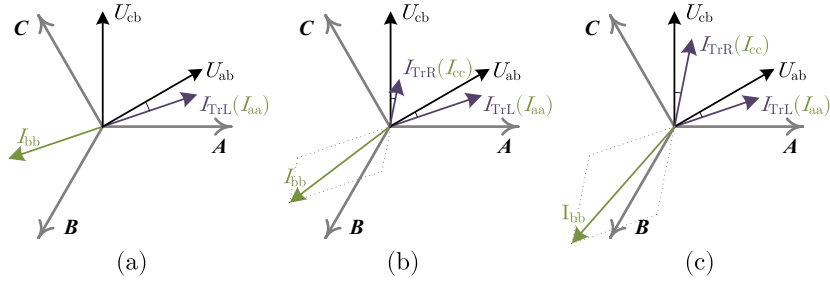


**Fig. 3.** Phasor diagrams (Vectors A, B and C represent the phase angles of the ideal three-phase grid voltage phasors  $\check{U}_A, \check{U}_B, \check{U}_C$ ) of a V/v transformer with different load conditions (a)  $I_{TL} = I_{Tr}$   $I_{TR} = 0$ ; (b)  $I_{TL} = I_{Tr}$   $I_{TR} = 0.5 I_{Tr}$ ; (c)  $I_{TL} = I_{Tr}$   $I_{TR} = I_{Tr}$

**Table 1.** Power quality of V/v transformer station

Load condition		Fig. 3(a)	Fig. 3(b)	Fig. 3(c)
Current unbalance factor		100%	77.2%	63.4%
Power factor	$pf_A$	0.979	0.979	0.979
	$pf_B$	0.667	0.667	0.95
	$pf_C$	NA	0.874	0.667

Assumption: traction load power factor  $pf_{Tr} = 0.95$

The current unbalance factor is defined in equation (3):

$$\varepsilon_I = \frac{|\check{I}^-|}{|\check{I}^+|} \times 100\%. \quad (3)$$

Negative sequence current will induce unbalance voltage in the grid and the definition of voltage unbalance ratio  $\varepsilon_U$  is similar to  $\varepsilon_I$  and can be estimated by equation (4):

$$\varepsilon_U = \frac{\sqrt{3} |\check{I}^-| U_L}{S_k} \times 100\%, \quad (4)$$

where  $U_L$  is the RMS value of the grid line to line voltage and  $S_k$  is the grid short-circuit capacity.

Besides the negative sequence issue, the reactive power problem is also evident in that currents are not in phase with three-phase grid voltage. Table 1 lists the current unbalance factor and power factors in different load conditions of the V/v transformer power supply.

The aforementioned issues all occur at the fundamental frequency (50 Hz), and there exist higher-order harmonics mainly generated by converters in the train. These harmonics can couple into the grid through transformers which cause extra losses and become a destabilizing factor. In the next two sections, an MMC-based cophase

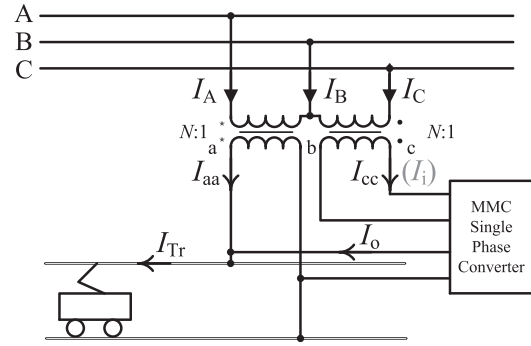


**Fig. 4.** V/v transformer with MMC-based cophase connection

supply scheme is presented to solve those problems and the neutral zone inside the station can be cancelled.

### 3. Compensation strategy design for a cophase power supply system

#### 3.1 Topology and full compensation

A back-to-back converter is connected between phases ab and cb to form a cophase supply scheme in Fig. 4. The positive direction of current value is defined by the arrows' direction.  $I_i$ ,  $I_o$  and  $I_{Tr}$  represent the current RMS values of the converter input current, converter output current and traction load current respectively. We assume that the transformer is ideal so that equation (1) holds true.



The first two equations in equation (5) still hold true and are expanded in equation (8):

$$\begin{aligned} I_{Tr} \cos(\phi_{Tr}) - I_{aa} \cos(\theta_{ab} + \varphi_A) \\ = I_{cc} \cos(120^\circ - \theta_{cb} - \varphi_C). \end{aligned} \quad (8)$$

As shown in Fig. 4, three-phase currents obey Kirchhoff's law, which leads to equation (9):

$$\check{I}_{aa} + \check{I}_{bb} + \check{I}_{cc} = 0. \quad (9)$$

Partial compensation relies on the grid code (according to National Grid report 'GC0088-Voltage Unbalance') about the limit of permissible voltage unbalance, and regulation for distribution network operators is often set at 2%. Phasors  $\check{I}_{aa}$ ,  $\check{I}_{bb}$  and  $\check{I}_{cc}$  contain six undetermined values (magnitude and phase angle of each phasor). We can decompose equation (9) into two constraints, as shown in equation (10), and convert these equations into equation (11):

$$\begin{aligned} \text{proj}_\alpha(\check{I}_{aa}) + \text{proj}_\alpha(\check{I}_{cc}) &= -\text{proj}_\alpha(\check{I}_{bb}) \\ \text{proj}_\beta(\check{I}_{aa}) + \text{proj}_\beta(\check{I}_{cc}) &= -\text{proj}_\beta(\check{I}_{bb}), \end{aligned} \quad (10)$$

where  $\text{proj}_\alpha$  projects the phasor to the  $\alpha$  axis which is aligned with phase A, and  $\text{proj}_\beta$  projects the phasor to the  $\beta$  axis which is  $90^\circ$  behind the A axis.

$$\begin{aligned} I_{aa} \cos(\varphi_A) - I_{cc} \sin(30^\circ - \varphi_C) &= I_{bb} \cos(60^\circ - \varphi_B) \\ -I_{aa} \sin(\varphi_A) + I_{cc} \cos(30^\circ - \varphi_C) &= I_{bb} \sin(60^\circ - \varphi_B). \end{aligned} \quad (11)$$

In addition to voltage unbalance limit, power factor has to be corrected above 0.9, implying  $\varphi_{A, (B, C)} \in (-25.8^\circ, 25.8^\circ)$ . So three constraints are imposed on the phase angles  $\varphi_{A, (B, C)}$ , leading to six constraints in total with equation (8) and equation (11) to explicitly formulate the desired current phasors  $\check{I}_{aa, (bb, cc)}$ . Finally, the RMS values of the transformer secondary side current are expressed in equation (12). So far, each current phasor in the system can be derived using the vector addition and subtraction operations illustrated in Fig. 6. We have thus shown that the desired compensation result can be achieved by setting a suitable set of

three-phase current phase angles.

$$\begin{aligned} I_{aa} &= 2I_{Tr} \cos(\phi_{Tr}) \cos(30^\circ - \varphi_B + \varphi_C) / \\ &\quad [2 \cos(\theta_{ab} + \varphi_A) \cos(30^\circ - \varphi_B + \varphi_C) + \\ &\quad \sin(\theta_{cb} - \varphi_A + \varphi_B + \varphi_C) - \\ &\quad \cos(30^\circ + \theta_{cb} + \varphi_A - \varphi_B + \varphi_C)] \\ I_{bb} &= I_{Tr} \cos(\phi_{Tr}) \csc(30^\circ + \varphi_B) \cdot \\ &\quad (\cos(30^\circ - \varphi_A - \varphi_B + \varphi_C) - \sin(\varphi_A - \varphi_B - \varphi_C)) / \\ &\quad [2 \cos(\theta_{ab} + \varphi_A) \cos(30^\circ - \varphi_B + \varphi_C) + \\ &\quad \sin(\theta_{cb} - \varphi_A + \varphi_B + \varphi_C) - \\ &\quad \cos(30^\circ + \theta_{cb} + \varphi_A - \varphi_B + \varphi_C)] \\ I_{cc} &= 2I_{Tr} \cos(\phi_{Tr}) \cos(30^\circ - \varphi_A + \varphi_B) / \\ &\quad [2 \cos(\theta_{ab} + \varphi_A) \cos(30^\circ - \varphi_B + \varphi_C) + \\ &\quad \sin(\theta_{cb} - \varphi_A + \varphi_B + \varphi_C) - \\ &\quad \cos(30^\circ + \theta_{cb} + \varphi_A - \varphi_B + \varphi_C)] \end{aligned} \quad (12)$$

The essence of partial compensation is to reduce the system costs, and we plan to reduce two types of costs: reducing construction costs by reducing the capacity of the cophase system, and reducing resistive losses to save on operational costs. These two objectives can be achieved using the partial compensation optimization procedure in Algorithm 1, and in our case study we consider a traction power supply system with the following defined parameters: current phase angle limit  $\varphi_{\text{limit}} = 25^\circ$ , grid short-circuit capacity  $S_k = 500\text{MVA}$ , traction load power factor  $\text{pf}_{Tr} \in [0.85, 1]$ , minimum traction load active power  $P_{\text{min}} = 1\text{MVA}$ , maximum traction load active power  $P_{\text{max}} = 30\text{MVA}$  and voltage unbalance limit  $\varepsilon_{U_{\text{limit}}} = 1.9\%$ .

As illustrated in Algorithm 1, the first step is to minimize the the current capacity under the maximum load condition with different load power factors. The optimal result of the first step is then fed to the second step to search for the optimal angles for the three-phase currents to minimize the resistive energy losses. To obtain the optimal solutions, this paper adopts an exhaustive search approach, where the search space for the power factor and the power capacity is segmented into small meshes with the mesh scale of  $1.25 \times 10^{-2}$  for the power factor and 1 MW for the power. The accuracy for the resultant phase angle of the three-phase currents  $[\varphi_A, \varphi_B, \varphi_C]$  is set to  $0.1^\circ$ .

Through exhaustive search, Algorithm 1 optimizes the converter size, resulting in  $I_{\text{max}} =$

### Algorithm 1 Partial compensation optimisation procedure

#### Initialisation:

Current phase angle limit  $\varphi_{\text{limit}}$ ;  
 Maximum voltage unbalance factor  $\varepsilon_{U_{\text{limit}}}$ ;  
 Grid short-circuit capacity  $S_k$ ;  
 Active power boundary of traction load  $P_{\text{min}}, P_{\text{max}}$ ;  
 Power factor boundary of traction load  $\text{pf}_{\text{min}}, \text{pf}_{\text{max}}$

#### Optimisation output:

Maximum RMS value of the conditioner  $I_{\text{max}}$ ;  
 Optimised phase angles  $[\varphi_A, \varphi_B, \varphi_C]$  for given traction active power  $P_{\text{Tr}}$  and power factor  $\text{pf}_{\text{Tr}}$ .

#### Step 1:

function CAPACITY REDUCTION( $P_{\text{max}}, \text{pf}_{\text{min}}, \text{pf}_{\text{max}}$ )

```

 $I_{\text{max}} \leftarrow \infty$ 
for  $\text{pf} = \text{pf}_{\text{min}}$  to  $\text{pf}_{\text{max}}$  do
    minimise  $\tilde{I}_{\text{max}} = \max(I_i, I_o)$ 
         $\varphi_A, \varphi_B, \varphi_C$ 
    subject to  $\max(|\varphi_A|, |\varphi_B|, |\varphi_C|) \leq \varphi_{\text{limit}}$ ,
         $I_{\text{Tr}} = P_{\text{max}}/U_{\text{ab}}/\text{pf}$ ,
         $\varepsilon_U < \varepsilon_{U_{\text{limit}}}$ 
    if  $\tilde{I}_{\text{max}} < I_{\text{max}}$  then
         $I_{\text{max}} \leftarrow \tilde{I}_{\text{max}}$ 
    end if
end for
return  $I_{\text{max}}$ 
end function
    
```

#### Step 2:

function STRATEGY SEARCH( $P_{\text{min}}, P_{\text{max}}, \text{pf}_{\text{min}}, \text{pf}_{\text{max}}, I_{\text{max}}$ )

```

for  $P_{\text{Tr}} = P_{\text{min}}$  to  $P_{\text{max}}$  do
    for  $\text{pf} = \text{pf}_{\text{min}}$  to  $\text{pf}_{\text{max}}$  do
        minimise  $I_1^2 + I_2^2$ 
             $\varphi_A, \varphi_B, \varphi_C$ 
        subject to  $\max(|\varphi_A|, |\varphi_B|, |\varphi_C|) \leq \varphi_{\text{limit}}$ ,
             $I_{\text{Tr}} = P_{\text{Tr}}/U_{\text{ab}}/\text{pf}$ ,
             $\varepsilon_U < \varepsilon_{U_{\text{limit}}}$ ,
             $\max(I_i, I_o) \leq I_{\text{max}}$ .
        Save strategy vector  $[P_{\text{Tr}}, \phi_{\text{Tr}}, \varphi_A, \varphi_B, \varphi_C]$ 
    end for
end for
return strategy matrix  $[P_{\text{Tr}}, \phi_{\text{Tr}}, \varphi_A, \varphi_B, \varphi_C]$ 
end function
    
```

471.33A with the maximum capacity 12.96MVA and  $k_{\text{size}} = 0.367$ . The maximum capacity is required when the load has the highest active power and the lowest power factor. In this case study, when the partial compensation scheme is applied,  $k_{\text{size}}$  is reduced by 27.9% (5MVA) compared with the full compensation scheme. Figure 7 shows the compensation ratios of apparent power and active power using full and partial compensation strategies.

The phase angles under different traction load conditions are illustrated in the three contour plots (Fig. 8). The target phase angles of three-phase current vary according to different traction load characteristics and there is no single optimal combination that suits all conditions. In several cophase conditioner studies [8,9], researchers only minimize the converter active power capacity

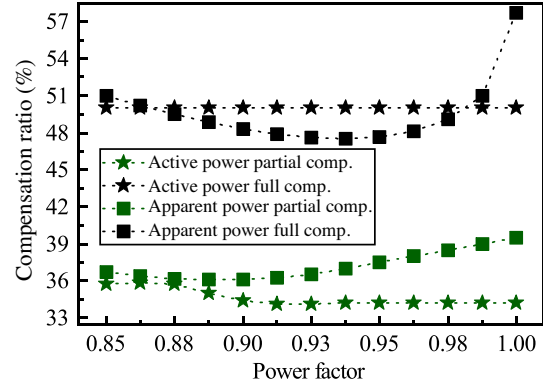


Fig. 7. Compensation percentage comparison: full compensation vs. partial compensation

under different loads, and this approach is equivalent to minimizing the current magnitude of the conditioner. Here in our studies, we assume that total operational losses are mainly resistive losses ( $P_{\text{loss}} \propto I^2$ ). Figure 9 illustrates the minimal resistive losses using our proposed optimization scheme when the total currents  $I_0^2 + I_1^2$  of both sides of the converter are minimized. In Fig. 9, z-axis values are normalized and the orange bars are the additional losses if the magnitude of output current is minimized (compared to our approach 'blue bars'). Figure 9 shows that the resistive losses are reduced significantly (18.7%) at unity power factor load, which is a typical characteristic for high-speed train traction drive systems.

Using the phase angles of three-phase current as the control objectives, the cophase controller can dynamically compensate the unbalanced current arising from the traction load such that the negative sequence component and the grid side power factor are corrected to the desired limits with the least resistive losses.

## 4 Modelling and control of the MMC-based power conditioner

In this section, a four-phase MMC back-to-back converter is used to implement the proposed cophase supply scheme. The converter topology is shown in Fig. 10(a), where phase a and phase b operate as a rectifier and phase e and phase f operate as an inverter.

### 4.1 Single-phase model and modulation

Each branch of the MMC phases is composed of many half-bridge modules ( $SM_1 \dots SM_N$ ) with floating capacitors connected in serial with an arm inductor ( $L_{\text{br}}$ ). Two identical branches form

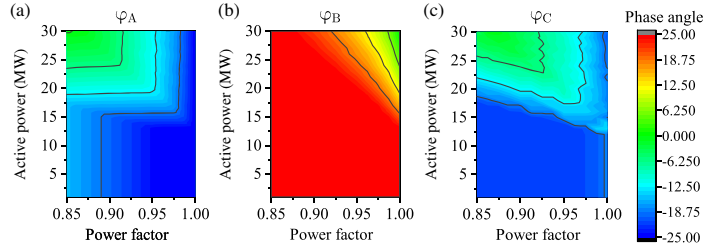


Fig. 8. Compensation strategy for different load conditions (a)  $\varphi_A$ ; (b)  $\varphi_B$ ; (C)  $\varphi_C$

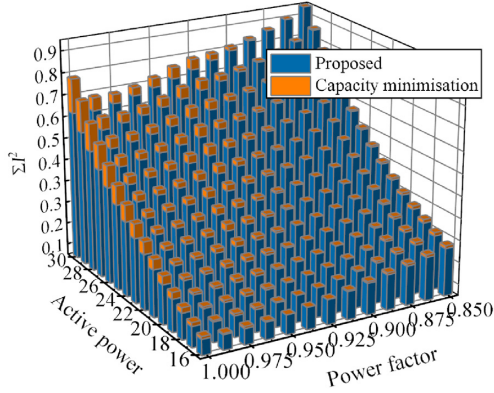


Fig. 9. Resistive losses comparison

one phase which can be simplified by an average model. In Fig. 10(b), modules in upper and lower branches are represented by controlled voltage sources  $u_u$  and  $u_l$  while  $u_s$  is the external voltage source. Assume the capacitor voltage is regulated to support stabilizing  $U_{dc}$ , according to Kirchhoff's law, then the circuit equations of upper and lower branches are:

$$u_s - L_s \frac{di_s}{dt} - R_s i_s + R_{br} i_u + L_{br} \frac{di_u}{dt} + u_u = \frac{U_{dc}}{2}, \quad (13)$$

$$u_s - L_s \frac{di_s}{dt} - R_s i_s - R_{br} i_l - L_{br} \frac{di_l}{dt} - u_l = -\frac{U_{dc}}{2}, \quad (14)$$

then add and subtract (13) and (14) yielding (15) and (16).

$$u_s = R_s i_s + L_s \frac{di_s}{dt} + R_{br} \underbrace{\frac{i_l - i_u}{2}}_{i_{dif}} + L_{br} \frac{d}{dt} \underbrace{\frac{i_l - i_u}{2}}_{i_{dif}} + \underbrace{\frac{u_l - u_u}{2}}_{u_{dif}} \quad (15)$$

$$\frac{U_{dc}}{2} = R_{br} \underbrace{\frac{i_u + i_l}{2}}_{i_{com}} + L_{br} \frac{d}{dt} \underbrace{\frac{i_u + i_l}{2}}_{i_{com}} + \underbrace{\frac{u_u + u_l}{2}}_{u_{com}} \quad (16)$$

Expressed in equations (15) and (16), the terminal voltage can be controlled by the differential-mode voltage between the upper and lower branches  $u_{dif} = (u_l - u_u)/2$ , and the dc-link voltage is maintained by the common-mode voltage  $u_{com} = (u_l + u_u)/2$ . Similarly, differential-mode current  $i_{dif} = (i_l - i_u)/2$  determines the output terminal current  $i_s$ , ( $i_s + i_u = i_l$ ), and common-mode current  $i_{com} = (i_l + i_u)/2$  represents the energy transfer between branches. Therefore, the terminal voltage and current are determined by the differential-mode values of two branches in each phase while, the internal states are controlled by the common-mode values.

The carrier wave phase-shifted ( $2\pi/N$ ) PWM method has been used for MMC modulation. Although the nearest level modulation (NLM) enjoys lower switching losses, the proposed 25-level converter does not have enough modules for direct NLM. All branches share the same phase-shifted carrier waves. These carrier waves are compared with the voltage reference to generate switching pulses to drive each half bridge.

#### 4.2 Current control and capacitor balancing

The rectifier side of the MMC draws current with the designed phase angle while stabilizing the average dc-link voltage. Meanwhile, the other two phases (phases e, f) inject current into the load for direct compensation. We assume that real-time phasor measurement of voltage and current at transformer secondary terminals is available with a one-unit sample time delay. The desired compensation current can be derived by the subtraction of current reference  $i_{aa}^{ref}$  (derived by equation (12)) and real measurement  $i_{Tr}$ . Figure 11 illustrates the procedure of reference current calculation for  $i_1^{ref}$  and  $i_o^{ref}$ .

In most recent literature, bang-bang control has been used for current tracking, but good tracking performance requires very narrow hysteresis width which results in unpredictable and high switching frequency. However, in reality, high

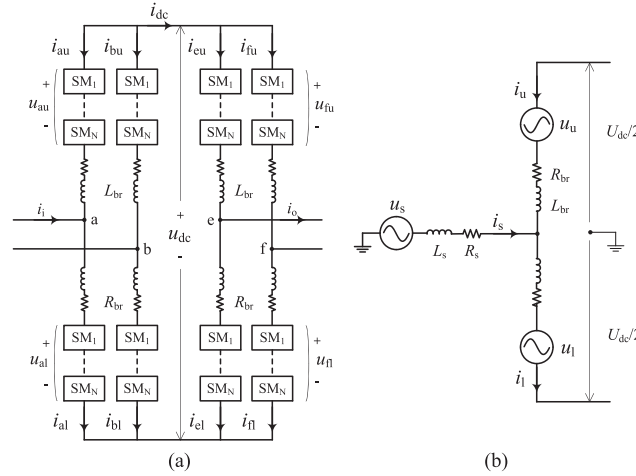


Fig. 10. MMC topology (a) and single-phase equivalent circuit (b)

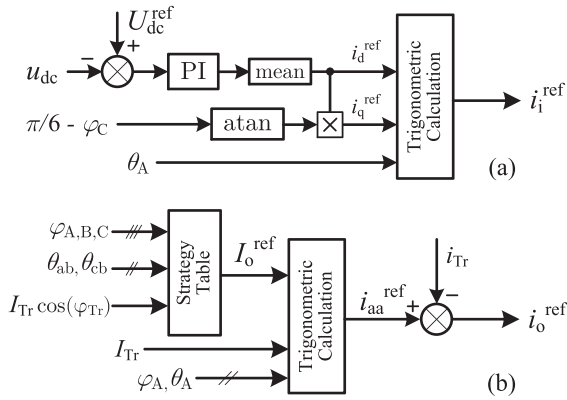


Fig. 11. Reference current design scheme (a)  $i_d^{\text{ref}}$ , (b)  $i_o^{\text{ref}}$

power switches cannot accept very high switching frequency.

Alternatively, we can either transform the single-phase current into a rotating dq frame with respect to the transformer terminal voltage and adopt two PI (proportional-integral) controllers, or directly use PR (proportional-resonant) controllers to track sinusoidal reference components. Based on the internal model principle, a PR controller is the combination of a proportional gain, a fundamental resonant term and harmonic compensator terms [10].

$$C_{\text{PR}}(s) = K_p + K_{r1} \frac{s}{s^2 + \omega_1^2} + \sum_{h=3,5,\dots} K_{rh} \frac{s}{s^2 + (\omega_1 h)^2} \quad (17)$$

The principal frequency components in the reference signal can be controlled by specifically designed resonant terms, and the residual component is controlled by the proportional term. In this

case, the fundamental component and the third-order harmonic have the largest portions, and a PR controller is designed as given in equation (18):

$$C_{\text{PR}}(z) = K_p + K_{r1} \frac{1}{\omega_1^2 T_{\text{sc}}} \frac{(1 - \cos(\omega_1 T_{\text{sc}})) z^2 + \cos(\omega_1 T_{\text{sc}}) - 1}{z^2 - 2 \cos(\omega_1 T_{\text{sc}}) z + 1} + K_{r3} \frac{1}{\omega_3^2 T_{\text{sc}}} \frac{(1 - \cos(\omega_3 T_{\text{sc}})) z^2 + \cos(\omega_3 T_{\text{sc}}) - 1}{z^2 - 2 \cos(\omega_3 T_{\text{sc}}) z + 1} \quad (18)$$

where the 'first zero hold' method is adopted for discretization, and  $\omega_1 = 100\pi$ ,  $\omega_3 = 300\pi$  and  $T_{\text{sc}}$  is the controller sampling time.

The capacitor voltage in each submodule cannot be guaranteed if we solely modulate the MMC for current tracking. A simple voltage balance scheme based on the proportional control is introduced by adding a small portion signal into the original voltage reference. Capacitors with lower voltage than average will turn on for a longer time during charging period, while capacitors with higher voltage than average will turn on for a longer time in the discharging period. The charging and discharging status is decided by the direction of the branch current.

Control diagrams of the current control and the voltage balancing are illustrated in Fig. 12, and each sub-module has an individual control signal added on the voltage reference for each branch. The composite references are compared with phase-shifted carrier wave to generate PWM signals for switches in phase a. The control schemes for the other phases are similar, but the differential-mode voltage reference has to be reversed in phases b and f.

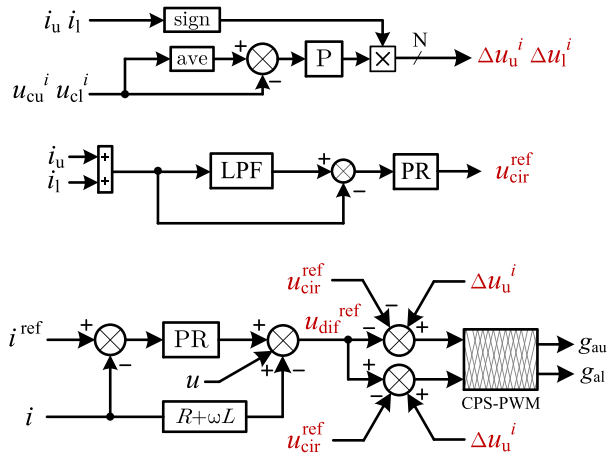


Fig. 12. Capacitor voltage balance control and current control

## 5 Simulation and performance analysis of the proposed scheme

### 5.1 System control scheme and simulation setup

A 25-level single phase back-to-back MMC is simulated for cophase conditioning; the system and simulation parameters are listed in Table 2. A control diagram of the whole system is presented in Fig. 13. Real-time phasor measurements of voltage/current at transformer/converter ports are assumed to be fully available. The compensation parameters are derived by linear interpolation of the strategy matrix based on instantaneous active and reactive traction power, and the parameters are updated at 100 Hz frequency. Then a series of MMC control actions are implemented accordingly. Two sets of simulations are designed to test the performance of the proposed cophase operation scheme for 20 MW static load and dynamic load varying from 0 MW to 30 MW.

Table 2. Simulation system parameters

Type	Parameter	Symbol	Value
Supply system parameter	Grid voltage	$V_{ph2ph}$	110 kV
	Short-circuit capacity	$S_k$	500 MVA
	X/R ratio		7
	Transformer ratio	N	110 kV/27.5 kV
MMC parameter	dc-link voltage	$V_{dc}$	48 kV
	Submodule number	$n_{sub}$	24
	Submodule voltage	$V_{sub}$	2 kV
	Submodule capacitor	$C_{sub}$	2 mF
	Branch inductor	$L_{br}$	30 mH
	Switching frequency	$f_{sw}$	500 Hz
Simulation parameter	Solver type		ode23t
	Simulation step	$T_s$	5 $\mu$ s
	Control sampling time	$T_{sc}$	100 $\mu$ s

### 5.2 Cophase supply for static load

We first discuss the performance of static load compensation where a controlled current source is used to simulate a 20 MW (pf = 0.95) static load. The load power and grid voltage unbalance are illustrated in Fig. 14; the power conditioner starts to compensate at 0.4 s. It is shown that the voltage unbalance ratio drops from 4.5% to 2% in 60 ms and finally settles to 1.95%. Three-phase grid voltages and currents are presented in Fig. 15. It is noticeable that the voltage amplitudes (green lines) have larger differences before the compensation is implemented but they are restored to approximately equal amplitude at 0.45 s. The grid side current  $I_C$  is almost zero before compensation (see Fig. 3a) and the three-phase currents remain unbalanced to some degree in partial compensation strategy. As shown in Fig. 16, which plots the power factor at the grid side, it is clear that the three-phase power factors are corrected above 0.9 with the proposed compensation.

The modern electrified railway rolling stocks are powered by ‘ac-dc’ or ‘ac-dc-ac’ conversion systems through traction drives where the converters inject harmonic currents into the power supply system. To investigate harmonic issues, rectifiers are modelled as several three-level single phase NPC (neutral-point clamped) converters with fixed load at dc side. These converters are connected in the railway power supply system through a step-down transformer. Single-phase rectifiers will naturally generate harmonic components which are used to represent the harmonics issue.

In the proposed control strategy, third-order harmonics (150 Hz) can be directly suppressed using the current reference signal design

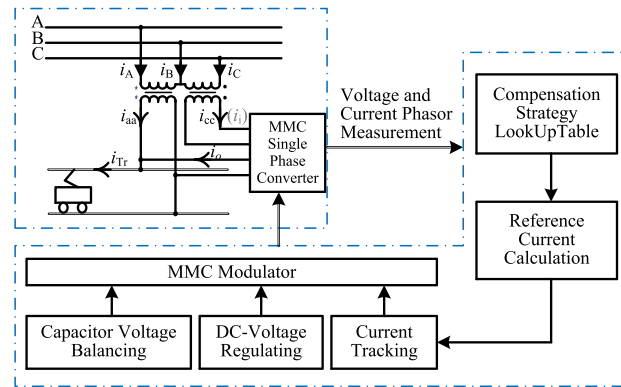


Fig. 13. Cophase system and control scheme diagram

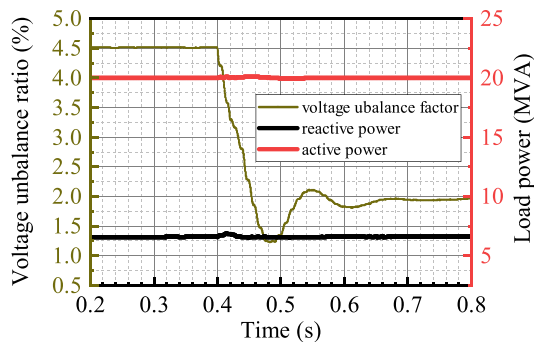


Fig. 14. Voltage unbalance factor under static load

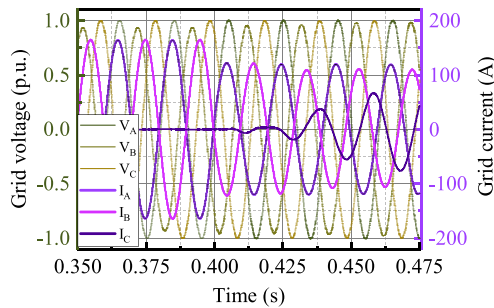


Fig. 15. Grid voltage and current under static load

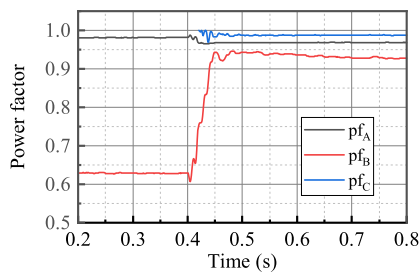


Fig. 16. Grid side power factor correction under static load

procedure. The MMC conditioner cancels most of the third-order harmonics and suppresses a few high-order harmonics as well. As illustrated in Fig. 17(a), the grid current  $I_A$  contains 4.38%

of third-order harmonics and some small ninth- and 11th-order harmonics before compensation. After the compensation starts, the third-order harmonic becomes neglectable and the remaining odd harmonics are all suppressed below 2.06%.

The MMC internal states including sub-module capacitor voltages and circulating currents ( $i_{com}$ ) in phase a and phase e are shown in Fig. 18. Due to the topology symmetry, phase b and phase f exhibit the same behaviour. The capacitor voltages in each submodule are balanced and the circulating currents have little oscillating components at steady state.

### 5.3 Cophase compensation for varying loads

In practice, rather than being constant, the load can vary drastically. For simplicity, the load is simulated by a controlled current source which delivers different active and reactive power at different time instants. Figure 19(a) illustrates the designed dynamic load profile: the active power increases from 0 MW to 30 MW during 0.1 s to 6 s, and decreases afterwards. The red line shows the designed profile of varying power factor.

The green line in Fig. 19(b) shows the voltage unbalance ratio. Although the load keeps changing, the voltage unbalance factor can be fully controlled below 2%. When the traction active power is below 15 MW, the proposed cophase system controls power factor while simultaneously meeting the voltage unbalance requirement. When the traction active power is above 15 MW, the voltage unbalance ratio is restricted to 1.9% deliberately. But the actual  $\varepsilon_U$  settles at 1.9942% in the test due to some modelling error and delays.

Traction loads can change rapidly in cases where multiple trains start or accelerate simultaneously. Figure 20 shows the grid voltage

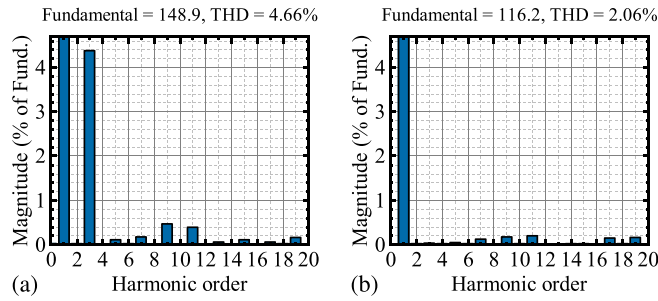


Fig. 17. FFT analysis of grid current  $I_A$  before and after compensation (static rectifier load) (a)  $I_A$  one cycle at 0.2s; (b)  $I_A$  one cycle at 0.8s

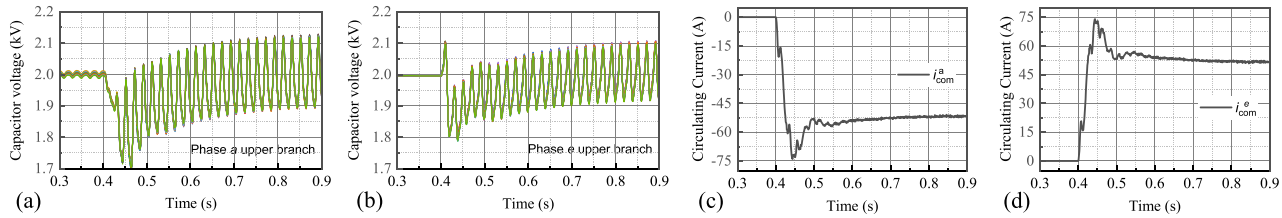


Fig. 18. MMC internal status: capacitor voltage (a) and (b), and circulating current (c) and (d)

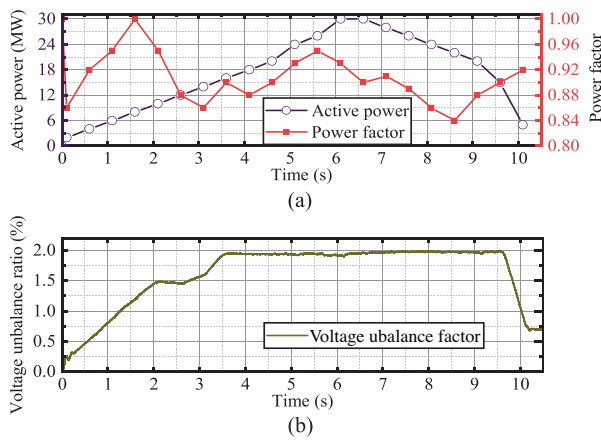


Fig. 19. Compensation for varying current source load (a) Varying load profile; (b) Voltage unbalance ratio

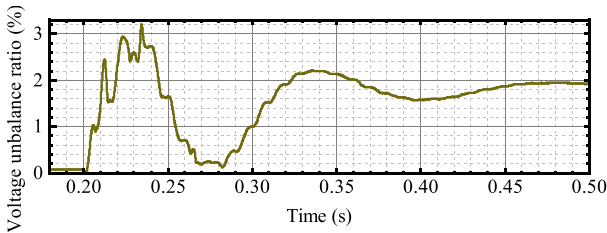


Fig. 20. Voltage unbalance under load step change

unbalance curve under a step load change where a 30 MW ( $pf = 0.85$ ) load is connected into the system at 0.2 s. This has led to an overshoot of 3.09% and a total duration of 67 ms of violating the grid code limit (2%). Because of the delay in load detection and compensation response, there is a oscillation during the first 50 ms after the step

change. Finally, voltage unbalance ratio is controlled within 2% after three grid cycles.

### 6 Conclusions

This paper has proposed a cophase supply conditioner using a 25-level modular multilevel single-phase back-to-back converter for power flow control. The conditioner is directly connected to the ports of V/v transformer for compensation of reactive power and unbalanced current and for low-order harmonics suppression. Phasor diagrams of the cophase system are analysed to derive the reference current for partial compensation which can be achieved by choosing suitable phase angles of the three-phase grid-side currents.

With the aim of minimizing the converter capacity and operation losses, a two-step strategy is designed. A case study shows that around 27.9% (5 MW) of capacity can be reduced by the partial compensation scheme for 30 MW traction load. And the conditioner operates with least resistive losses under dynamic traction load. While a variable impedance unit like MSVC can be used to further reduce converter capacity, this compensation strategy design is still applicable for the whole conditioning system design.

The optimized grid side current phase angles are chosen as the control strategy for real-time reference current calculation, and PR controllers are adopted for current tracking rather than bang-bang control used in the previous works. The

current signals have very little harmonics content, with 500 Hz switching frequency modulated by CPS-PWM.

Simulation results confirm that the proposed cophase conditioner can regulate voltage unbalance within 40 ms even in the worst scenario (load step change from zero to maximum). When the load is changing continuously without a large step change, the negative sequence component can be perfectly controlled. Third-order and other low-order harmonics induced by traction line converters can be effectively suppressed by MMC conditioner with the proposed control scheme.

There exists a small error in the steady state compensation performance, and the model used for control strategy design and reference calculation assumes an unlimited grid source and ideal transformers. However, in real applications, there exists non-negligible leakage inductance in the transformer and the grid capacity is finite. These can be tackled by upgrading the control strategy in this cophase compensation system to accommodate more realistic conditions.

*Conflict of interest statement.* None declared.

## References

1. Hu H, Shao Y, Tang L, et al. Overview of harmonic and resonance in railway electrification systems. *IEEE Transactions on Industry Applications* 2018; **54**:5227–45.
2. Ogunsola A, Mariscotti A. *Electromagnetic Compatibility in Railways: Analysis and Management*, vol. 168. Springer-Verlag Berlin Heidelberg; 2012.
3. Luo A, Wu C, Shen J, et al. Railway static power conditioners for high-speed train traction power supply systems using three-phase V/V transformers. *IEEE Transactions on Power Electronics* 2011; **26**:2844–56.
4. Luo A, Ma F, Wu C, et al. A dual-loop control strategy of railway static power regulator under V/V electric traction system. *IEEE Transactions on Power Electronics* 2011; **26**: 2079–91.
5. Lao KW, Dai N, Liu WG, et al. Hybrid power quality compensator with minimum DC operation voltage design for high-speed traction power systems. *IEEE transactions on power electronics* 2012; **28**:2024–36.
6. Lao KW, Wong MC, Dai N, et al. A systematic approach to hybrid railway power conditioner design with harmonic compensation for high-speed railway. *IEEE Transactions on industrial electronics* 2014; **62**:930–42.
7. Chen B, Zhang C, Zeng W, et al. Electrical magnetic hybrid power quality compensation system for V/V traction power supply system. *IET Power Electronics* 2016; **9**:62–70.
8. Chen M, Li Q, Roberts C, et al. Modelling and performance analysis of advanced combined co-phase traction power supply system in electrified railway. *IET Generation, Transmission & Distribution* 2016; **10**:906–16.
9. Chen B, Zhang C, Tian C, et al. A hybrid electrical magnetic power quality compensation system with minimum active compensation capacity for V/V cophase railway power supply system. *IEEE Transactions on Power Electronics* 2015; **31**:4159–70.
10. Zhong QC, Hornik T. *Control of Power Inverters in Renewable Energy and Smart Grid Integration*, vol. 97. John Wiley & Sons Ltd, The Atrium, Southern Gate, Chichester, West Sussex, PO19 8SQ, United Kingdom, 2012.